Journal of the Korean Physical Society (2021) 79:734–740
https://doi.org/10.1007/s40042-021-00273-1

Online ISSN 1976-8524
Print ISSN 0374-4884

ORIGINAL PAPER - CONDENSED MATTER

Semimetallic nature of and magnetic polarons in EuB_6 studied using angle-resolved photoemission spectroscopy

Chul-Hee Min[1] · Boyoun Kang[2] · Beong Ki Cho[2] · En-Jin Cho[3] · Byeong-Gyu Park[4] · Hyeong-Do Kim[5]

Received: 30 June 2021 / Accepted: 14 July 2021 / Published online: 19 August 2021

Abstract
Temperature-dependent angle-resolved photoemission spectroscopy (ARPES) was carried out on single-crystalline EuB_6 samples. By measuring ARPES spectra in an extended Brillouin zone, we clearly observed a B 2*p* hole pocket centered at the *X* point, thus proving the semimetallic nature of EuB_6. Below the Curie temperature T_C, ARPES spectra show two B 2*p* bands of which separation is due to an exchange interaction between local Eu 4*f* and itinerant B 2*p* electrons. The exchange splitting becomes smaller as the temperature increases and disappears well above T_C. Additionally, a diffuse structure near the Fermi level survives at temperatures just above T_C. Such behavior is well described by using Monte Carlo simulations of a Kondo-lattice model, thus supporting the formation of magnetic polarons in EuB_6, which accounts for the resistivity upturn slightly above T_C as the temperature is lowered.

Keywords EuB_6 · Semimetal · Magnetic polaron · Angle-resolved photoemission spectroscopy

1 Introduction

The low-carrier-density system EuB_6 has long attracted much attention, because it shows an anomalous resistivity behavior concomitant with its ferromagnetic (FM) phase transition near its critical temperature (T_C) of 15.5 K [1]. In addition, another phase transition related to electronic excitations has been revealed in the FM phase by specific-heat and optical reflectivity measurements [2]. The low carrier density has been proposed to be essential to stabilize the FM order in a Kondo-lattice system [3]. According to the local-density approximation (LDA) or LDA+*U* band calculations [4–6], the Eu 5*d* and the B 2*p* bands overlap each other and form small electron and hole pockets, respectively, centered at the *X* point in the Brillouin zone (BZ), to produce low-density carriers. This picture is experimentally supported by Shubnikov-de Haas and de Haas-van Alphen (dHvA) measurements [7, 8], optical conductivity [9, 10], Andreev reflection spectroscopy [11], and resonant inelastic X-ray scattering [12]. On the other hand, *GW* calculations for another divalent hexaboride CaB_6 show an energy gap at the *X* point [13], which was confirmed using angle-resolved photoemission spectroscopy (ARPES) [14, 15], though it had been predicted to be semimetallic by LDA calculations [13, 16]. ARPES spectra of EuB_6 obtained by Denlinger et al. also show a bulk band gap at the *X* point [14]. Tunneling measurements also seem to provide evidence for a bulk band gap of 43 meV [17]. However, ARPES measurements on CeB_6 show an overlap of the Ce 5*d* and the B 2*p* bands at the *X* point, which is well described by theoretical bulk band structure [18]. Furthermore, recent ARPES studies on EuB_6 focused on its topological properties show a negligible gap in the paramagnetic (PM) phase and a clear semimetallic feature in the FM phase [19, 20]. Thus, some results on the origin of the low-density carriers in EuB_6 are controversial.

✉ Hyeong-Do Kim
hdkim6612@postech.ac.kr

1 Institut für Experimentelle und Angewandte Physik, Christian-Albrechts-Universität zu Kiel, 24098 Kiel, Germany

2 School of Material Science and Engineering, Gwangju Institute of Science and Technology, Gwangju 500-712, South Korea

3 Department of Physics, Chonnam National University, Kwangju 500-757, South Korea

4 PLS-II Beamline Division, Pohang Accelerator Laboratory, Pohang 37673, South Korea

5 XFEL Beamline Division, Pohang Accelerator Laboratory, Pohang 37673, South Korea

Another interesting issue involving EuB_6 is that when the temperature is decreased, the resistivity shows an upturn at a temperature of about 30 K and rapidly decreases down to a temperature of about 10 K [1, 21], which seems to be related with two consecutive transitions in the FM phase [2]. All the results from Raman spectra [22, 23], neutron scattering [24], field-dependent resistivity and magnetization measurements [25], muon-spin rotation measurements [26], electron-spin resonance measurements [27], nonlinear Hall effects [28], and fluctuation spectroscopy and weak nonlinear transport measurements [29] suggest that the phase transition at T_C is due to an overlap of bound magnetic polarons (MPs), thus inducing a percolative transition in the resistivity. Theoretical investigations based on a Kondo-lattice model also suggest the formation of bound MPs [30], and can reproduce both the resistivity anomaly and the consecutive transitions, though the lower temperature transition is percolative [31].

In this work, we present APRES results for $Eu_{1-x}La_x B_6$ in an extended BZ to observe the B $2p$ band crossing the Fermi level (E_F). Our data confirm the semimetallic nature of EuB_6, thus resolving the issue of the origin of the low-density carriers. Furthermore, temperature-dependent ARPES spectra show two clear exchange-split bands in the FM phase and an exchange-driven diffuse structure near E_F even in the PM phase. Such a structure is explained using a two-dimensional (2D) Kondo-lattice model, which shows MPs at temperatures slightly above T_C.

2 Experiments

Single-crystalline samples of $Eu_{1-x}La_xB_6$ ($x = 0.0$ and 0.2) were grown by using an Al flux method [32] and mounted on sample holders for ARPES on which their orientations were determined by their rectangular shapes or Laue pictures. ARPES measurements with a Scienta-SES2002 electron analyzer were carried out at the 4A1 μ-ARPES Beamline of PLS-II at Pohang Accelerator Laboratory. All samples were cleaved in situ to show a flat (001) surface by using a top-post method in a vacuum better than 7×10^{-11} Torr. Photon energies from 100 to 150 eV were used to probe a three-dimensional (3D) electronic structure, and no noticeable change was observed during the measurements. The total energy and momentum resolutions were set to be about 100 meV and 0.01 Å^{-1}, respectively, and E_F was determined from the Fermi edge of a Au film electrically connected to the samples. Sample temperature was lowered using an open-cycle liquid-He cryostat and controlled within 0.1 K using a resistive heater.

Because of a complicated issue related to the surface electronic structure of EuB_6 in ARPES spectra [14], we first investigated the electronic structure of electron-doped $Eu_{0.8}La_{0.2}B_6$. The number of electron carriers in $Eu_{0.8}La_{0.2}B_6$ is so large that its electronic structure may not be affected very much by surface defects as in a low-carrier-density system. According to the previous ARPES studies [14], the inner potential of EuB_6 was found to be about 11.2 eV, which renders a value of $h\nu = 130$ eV to reach the Γ point in the region of $h\nu = 100 \sim 150$ eV. Figure 1(a) shows the Fermi-surface (FS) map of $Eu_{0.8}La_{0.2}B_6$ at $h\nu = 130$ eV, which shows a

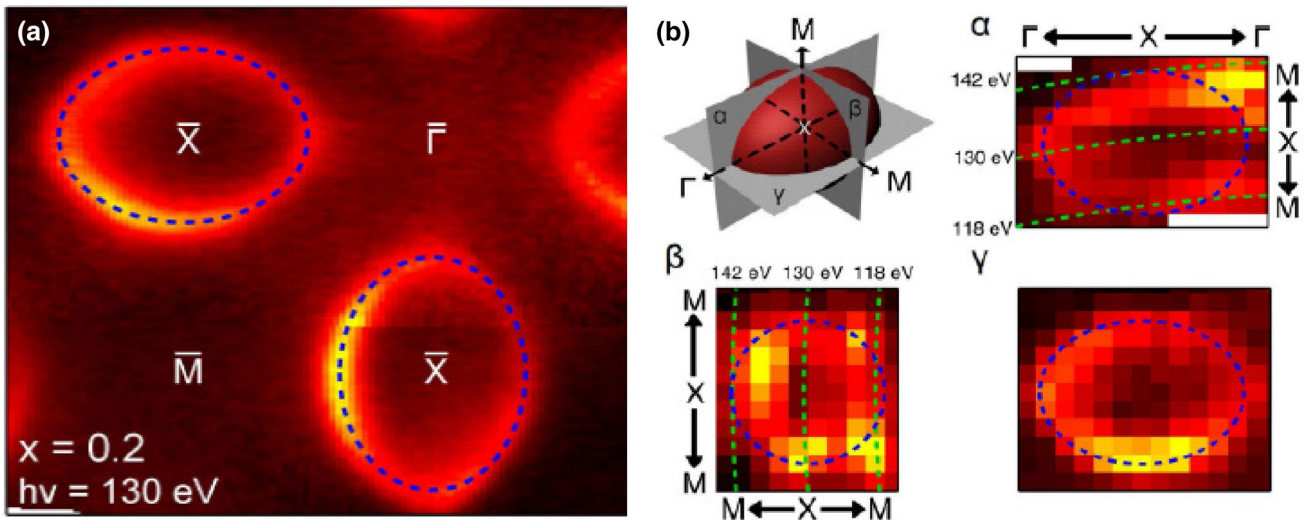

Fig. 1 **a** FS map of $Eu_{0.8}La_{0.2}B_6$ taken at $h\nu = 130$ eV and $T = 40$ K. **b** Cross-sectional FS maps of the same sample taken from $h\nu = 115$ to 146 eV. ARPES spectra are measured along the green dashed lines at each photon energy, and blue dashed elliptical guidelines for the FSs are of the same size

large elliptical electron pocket centered at the $\overline{X}$ point projected onto the surface BZ. To see how closely $h\nu = 130$ eV accesses the X point, we obtained FS maps by varying the photon energy from 115 to 146 eV, the results of which are shown in Fig. 1b. FS maps denoted by α, β, and γ are the cross-sectional views of the 3D ellipsoidal FS as shown in the upper left drawing. Because α and γ are for the same symmetry plane ΓXM, they should be the same, but the FS shape of α looks a little distorted when compared to that of γ (see blue dashed guidelines for the FSs). This may originate from a 3D artifact and strong matrix-element effects in ARPES spectra, which is especially strong near the FS edges in α along the surface normal direction. A Eu $4d \rightarrow 4f$ resonance at $h\nu > 135$ eV, which enhances enormously the Eu $4f$ peak at 1.5 eV, may also distort near-E_F features. Nevertheless, from these results, we can see that ARPES spectra at $h\nu = 130$ eV provide information on the electronic structure fairly close to the X point, and because of its 3D nature, we cannot account for its electronic structure by a surface state.

Regarding the issue of the bulk band gap between the Eu $5d$ and the B $2p$ bands at the X point [14], we investigated ARPES spectra of $Eu_{0.8}La_{0.2}B_6$ around the X point, but observing the B $2p$ band was difficult, which may have been due to the matrix-element effect in ARPES and strong Eu $4f$ signals near the Eu $5d$ band minimum. Thus, we measured ARPES spectra in a more extended BZ and show the results in Fig. 2. Figure 2a is again its FS map, and $\overline{\Gamma}^{(n)}$, $\overline{X}^{(n)}$, and $\overline{M}^{(n)}$ denote the nth nearest high symmetry points with respect to the sample surface normal. As we can clearly see in the map, the intensities around the $\overline{X}^{(1)}$ and the $\overline{X}^{(2)}$ points are much different from each other. Figure 2b is a constant-energy map at the binding energy (E_B) of 0.7 eV, which shows a striking difference not only in its intensity but also in shape, i.e., we can see a hollow spot at $\overline{X}^{(1)}$ but an intense one at $\overline{X}^{(2)}$.

To see the origin of these differences, we obtained ARPES spectra along the green dashed line in Fig. 2a and b and presented the results in Fig. 2c. Because Eu^{2+} $4f$-peak signals are two orders of magnitude larger around $E_B = 1.5$ eV than Eu $5d$ and B $2p$ ones [33], clear identification of the Eu $5d$- and the B $2p$-band dispersions in a usual ARPES-intensity plot is quite difficult. Thus, we presented them in a log scale by taking the logarithm of the ARPES intensity of a momentum distribution curve (MDC) after dividing by its minimum. Then, we can not only enhance very low ARPES signals but also effectively remove momentum-independent ones, especially the tails of the Eu $4f$ peaks. As is clear in the figure, near the $\overline{X}^{(1)}$ point, only the Eu $5d$-band signals are dominant and no sign of the B $2p$ band is observed. In contrast, near the $\overline{X}^{(2)}$ point, the B $2p$-band signals are stronger than the Eu $5d$ ones. Thus, we can conclude that ARPES spectra should, at least in our ARPES geometry and at $h\nu = 130$ eV, be taken around the $\overline{X}^{(2)}$ point to observe correctly the B $2p$ band dispersion.

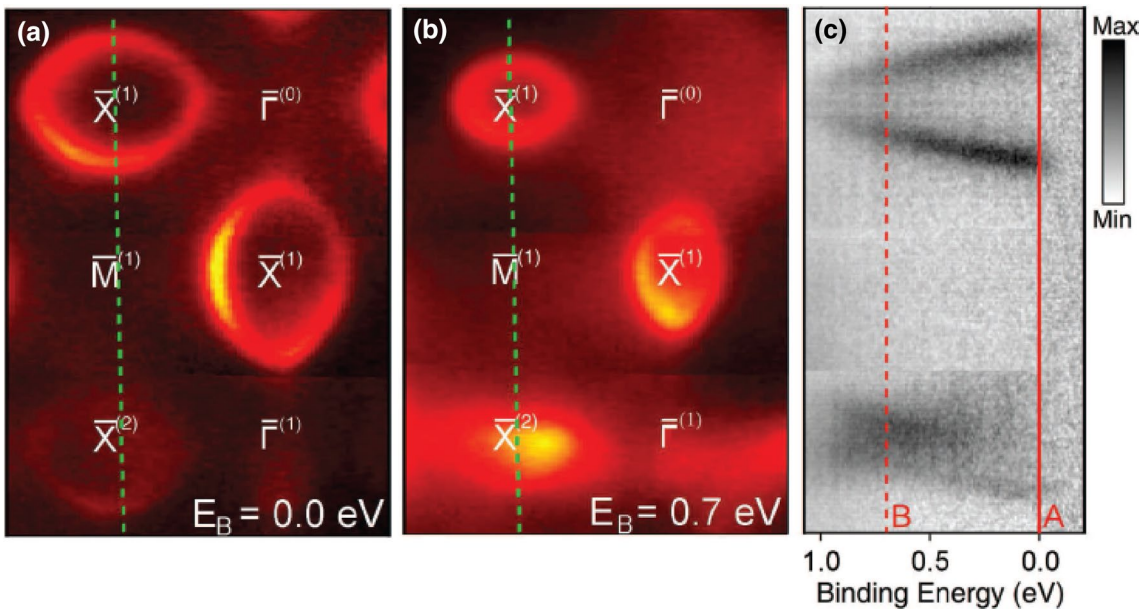

Fig. 2 **a** FS map of $Eu_{0.8}La_{0.2}B_6$ in an extended BZ. $\overline{\Gamma}^{(n)}$, $\overline{X}^{(n)}$, and $\overline{M}^{(n)}$ denote the nth nearest high-symmetry points with respect to the normal direction of the sample surface. **b** Same as in **a**, but a constant-energy-surface map taken at $E_B = 0.7$ eV. **c** Log-scale ARPES spectra along the green dashed line in **a** and **b**. The red solid and dashed lines denoted by A and B show where the maps **a** and **b** are obtained, respectively

Another interesting point is that the B 2*p* band overlaps by about 0.6 eV the Eu 5*d* band around $E_B = 0.7$ eV, which strongly suggests that intrinsic EuB_6 should be a compensated semimetal if both bands are rigidly shifted by La doping. Recent, ARPES measurements of CeB_6 also show a similar overlap of the Ce 5*d* and the B 2*p* bands at the *X* point, which is well described by theoretical bulk band structure [18], thus strengthening our argument.

3 Fermi surface and B 2*p* band

Figure 3a shows the FS map of EuB_6 in the PM phase at $T = 40.7$ K. As expected, we can observe a weak electron pocket around the $\overline{X}^{(1)}$ point (Eu 5*d* signals vanish when approaching the $\overline{X}^{(1)}$ point as seen in Fig. 2c), the size of which is nearly half that obtained by band calculations for an antiferromagnetic (AFM) phase to mimic the PM one [6]. Around the $\overline{X}^{(2)}$ point is seen a more intense spot in contrast to Fig. 2a, which implies that its character is different from that around the $\overline{X}^{(1)}$ point. The FS map of EuB_6 is quite similar to the map in Fig. 2b. Figure 3b is a log-scale ARPES image measured along the green dashed line in Fig. 3a and unambiguously shows that the B 2*p* band crosses E_F. Thus, together with the result around the $\overline{X}^{(1)}$ point, we can conclude that intrinsic EuB_6 is a compensated semimetal in which the Eu 5*d* and the B 2*p* bands overlap each other at the *X* point.

4 Temperature-dependent ARPES spectra

To examine the electronic-structure change of EuB_6 across the FM transition, we obtained temperature-dependent ARPES spectra along the green dashed line in Fig. 3a and present the results of the upper panels in Fig. 4. Yellow dashed lines are drawn as parabolas with an effective mass of 0.19 m_e and match the peak positions in the energy distribution curves and MDCs. The effective mass is also comparable to the value of 0.25 m_e obtained from dHvA measurements obtained on the minor axis of an elliptical hole pocket [7]. To confirm the spectral behavior described below, we also present MDCs taken at $E_B = 0.0$ and 0.3 eV in the lower panels of Fig. 4.

As the temperature is decreased to near T_C ($\sim$ 15.5 K), we can observe that the maximum of the B 2*p* band gradually shifts downward, leaving a diffuse structure near E_F denoted as red triangles. This behavior is more clearly seen in the lower panels in which the peaks denoted by red triangles become stronger with decreasing temperature. Peak positions for the down-shifted band are denoted by blue triangles. At $T = 15.7$ K and $E_B = 0.3$ eV, we can see a shoulder, denoted by a red triangle, that seems to form a band at temperatures below T_C. At temperatures well below T_C, this structure forms a well-defined band that shows dispersion similar to that of the down-shifted band. The separation between the two bands is about 0.35 eV, the origin of which should be the exchange interaction between the valence band and the local 4*f* moments that have an FM order, as observed in the ARPES spectra of Gd metal [34]. Because the B 2*p*

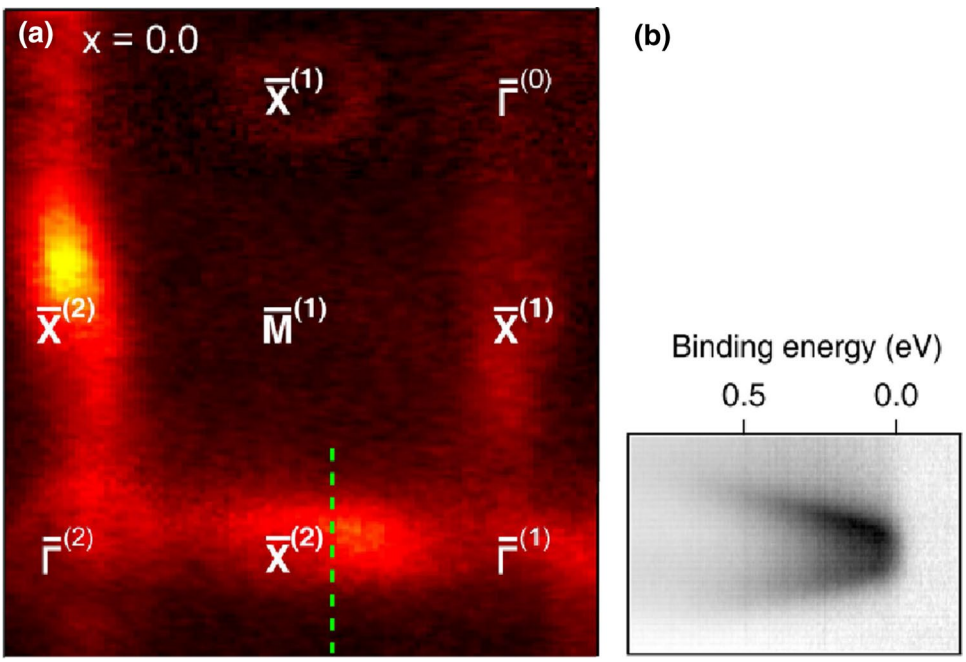

Fig. 3 **a** Same as in Fig. 2a but the sample is EuB_6. Interestingly, the FS map is quite similar to the constant-energy map in for $Eu_{0.8}La_{0.2}B_6$ Fig. 2b. **b** Log-scale ARPES spectra along the green dashed line in **a**

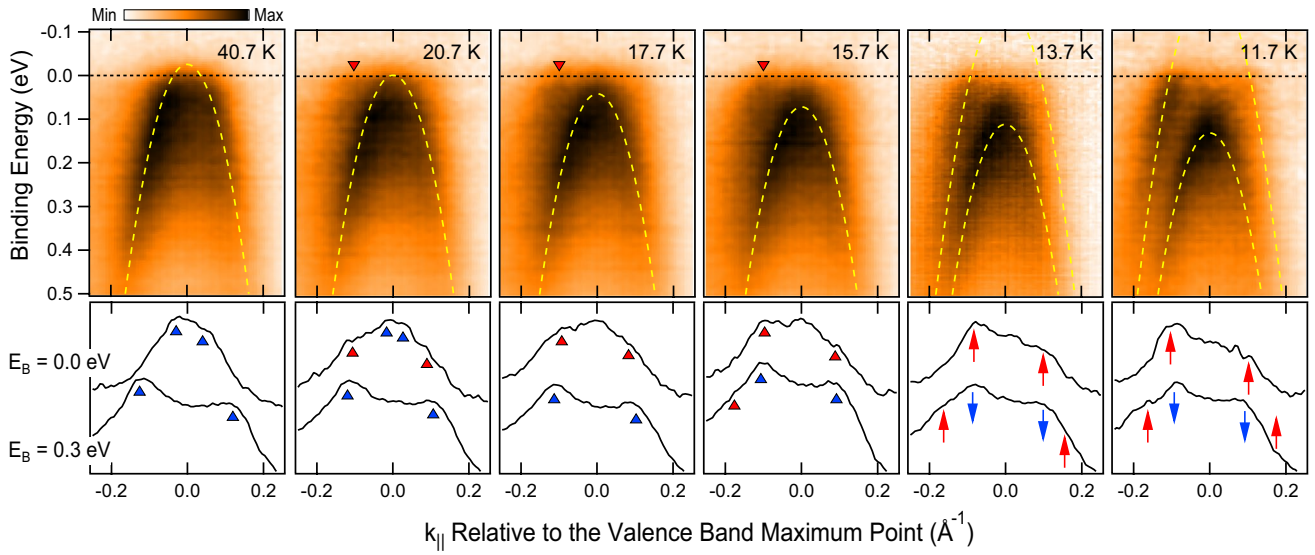

Fig. 4 Upper panels: Log-scale ARPES spectra of EuB_6 along the green dashed line in Fig. 1a for various temperatures from 40.7 to 11.7 K. Red triangles indicate spectral features which may be related to MPs, and yellow dashed parabolas are guidelines with an effective mass of 0.19 m_e. Lower panels: MDCs taken at $E_B = 0.0$ and 0.3 eV to show spectral features in the upper panels more clearly. Red triangles are peak positions for MPs, blue triangles for a merged band, and red/blue arrows for an exchange-split majority/minority band

band has an AFM Kondo coupling to the Eu 4*f* states [5], we can assign the upper/lower band as the majority/minority-spin band denoted by red/blue arrows in the lower panels, and we find their separation to be comparable to theoretical estimates [5, 6].

Returning to the diffuse structure near E_F above T_C, we can see that it is a vestige of the exchange-split majority-spin band and eventually merges with the minority one at $T = 40.7$ K. Because the separation of the exchange-split bands should be proportional to the sample magnetization [35, 36], if the density of itinerant electrons is spatially uniform, even when there are FM islands in the PM phase, no difference between spin-up and -down electrons should be observed by symmetry, i.e., no exchange splitting. However, with a small FM island, B 2*p* majority/minority-spin electrons feel a local repulsive/attractive potential caused by AFM exchange interactions and may form a (virtual) anti-bound/bound state, i.e., an MP, which mainly resides near the B 2*p*-band maximum/minimum in the BZ, if the potential is not so strong as in our case where the exchange interaction is an order of magnitude smaller than the B 2*p*-band width. Then, in ARPES spectra of the majority-spin band near the *X* point, we expect a diffuse anti-bound state and a slightly down-shifted band, the separation between which increases as the size of the FM island does, while in other *k* region, we expect the separation between the majority- and minority-spin bands to be negligible. In the PM phase, this behavior should take place both in the majority- and minority-spin bands, and the ARPES features at temperatures above T_C in Fig. 4 can be qualitatively explained using this scenario.

5 Monte Carlo simulations of a Kondo-lattice model

To see the above temperature-dependent spectral behavior is consistent with theoretically proposed MP formation, we calculated ARPES spectra using a 2D Kondo-lattice model [31]

$$H = -t \sum_{\langle i,j\rangle\sigma} c^{\dagger}_{i\sigma} c_{j\sigma} - J \sum_{i} \vec{\sigma}_i \cdot \vec{S}_i, \tag{1}$$

where $c^{\dagger}_{i\sigma}$ creates a conduction electron with spin σ at site i, and $\vec{\sigma}_i$ and $\vec{S}_i$ are the spins of a conduction electron and a local magnetic moment, respectively. t is a nearest-neighbor conduction-electron hopping parameter and J an exchange coupling between the conduction-electron spin and the local moment. $\langle i,j\rangle$ denotes a nearest-neighbor pair in the 2D square lattice. Though EuB_6 is a 3D system, the dimensionality may not be so important, because, as shown below, the size of a MP is less than 10 unit cells. For the local moments, Ising spins ($\vec{S}_i = \pm 1/2\hat{z}$) are assumed to diagonalize exactly the model Hamiltonian for a large-size lattice. To mimic the B 2*p* band dispersion at E_F and the exchange splitting, we assumed, in contrast to the authors of Refs. [30, 31], $t = 1$ eV and $J = 1.2$ eV, which belongs to the weak-coupling regime . To have a similar FS volume, we performed calculations for a 1% hole-doped system.

The model Hamiltonian was solved using the Monte Carlo method with the Metropolis algorithm for a $N \times N$ 2D square lattice ($N = 40$) with an open boundary condition

for a better momentum resolution than with a periodic one. Figure 5a shows local-moment distributions on the lattice at several temperatures, which was averaged over N^2 configurations after equilibrium had been reached, and Fig. 5b shows their average values S_{av} according to the temperature.

We can see that the FM transition occurs around $T/t = 0.0075$, which is not sharply defined because of finite-size effects. Interestingly, even when T is two times larger than T_C, the averaged local moment at each lattice site is far from zero and spin-up or spin-down FM islands with sizes of about five unit cells are observed. Figure 5c shows hole-density distributions corresponding to Fig. 5a. For $T > T_C$, the holes are both on spin-up or spin-down FM islands. However, for $T < T_C$, they are mainly on spin-down FM islands, which can be understood using the AFM Kondo coupling between the conduction-electron spin and the local moment, which results in partially unoccupied spin-up and fully occupied spin-down bands. For comparison, a hole-density distribution at $T = 0$ is shown in Fig. 5d, in which the holes are not uniformly distributed because of the open boundary condition, but do not form a highly concentrated island as in Fig. 5c. All these facts strongly suggest that, in this model system, MPs are robust at temperatures slightly above T_C .

Figure 5e shows snapshots of ARPES images near the conduction-band maximum corresponding to Fig. 5a. For comparison with the experimental data in Fig. 4, they are plotted symmetrically in $k_{\|}$. At high-enough temperature, we can see a single band crossing E_F, and at temperatures well below T_C, we can see two exchange-split bands with near-uniform separation for all momenta. As the temperature is increased, the separation becomes nonuniform, i.e., at $T/t = 0.0070$, it is much smaller well below E_F than around the conduction-band maximum, and at $T/t = 0.0078$, it vanishes well below E_F and leaves a distinctive structure around E_F. To see this spectral behavior more clearly, in Fig. 5f, we depicted energy distribution curves at $k_{\|} = 0$, and $9\pi/41$ relative to the conduction-band-maximum momentum. All these calculated spectral features are quite similar to the experimental ones in Fig. 4 and consistent with the qualitative argument in the previous section; thus, the spectral behavior in ARPES spectra at temperatures above T_C can be explained by MP formation.

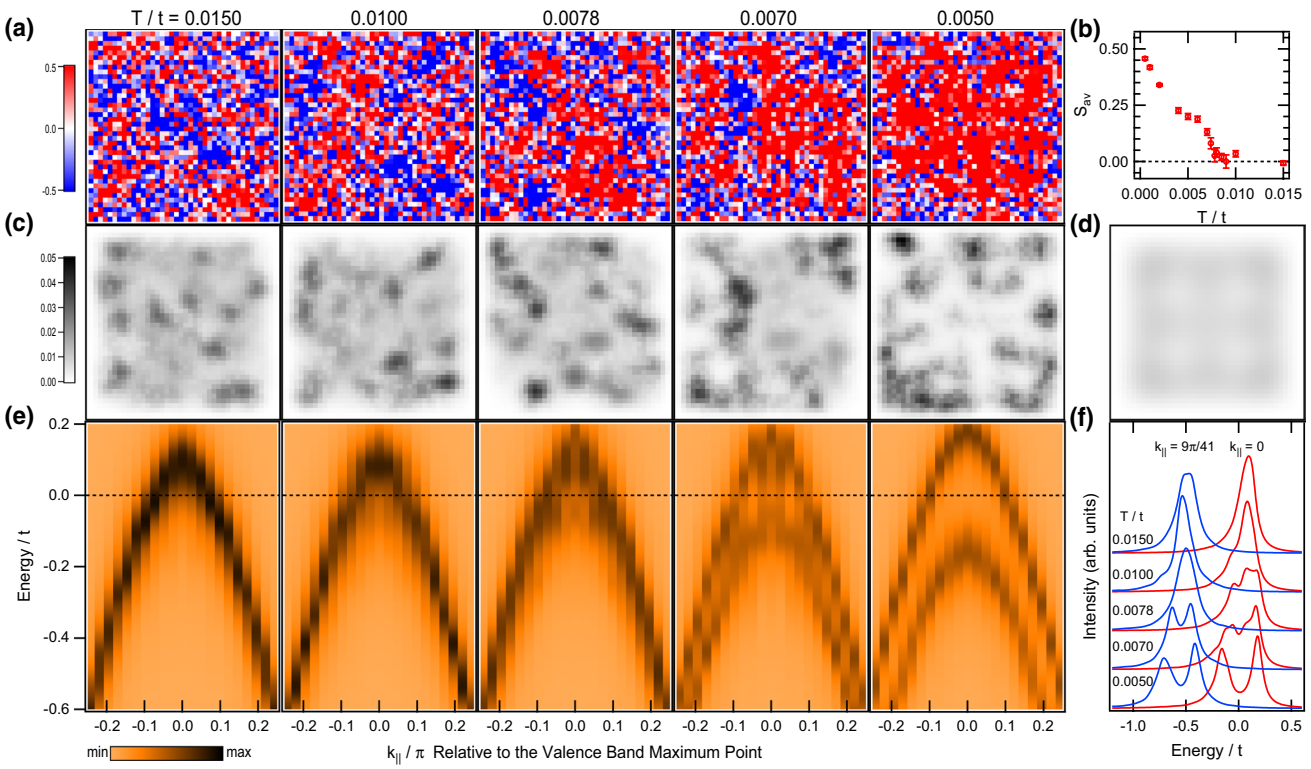

Fig. 5 Results of Monte Carlo simulations for a 1%-hole-doped 40×40 2D square Kondo-lattice model with an open boundary condition: **a** local-moment distributions on the lattice according to the temperature averaged over 1600 configurations after equilibrium had been reached. **b** Average of local moments according to the temperature, which shows $T_C \sim 0.0075t$. **c** Hole-density distributions corresponding to **a**. **d** Ground-state conduction-hole distribution at $T = 0$. **e** Snapshots of ARPES images near the conduction-band maximum corresponding to **a**. ARPES spectra are broadened by a Lorentzian with a $0.1t$ full width at half maximum. **f** Energy distribution curves at $k_{\|} = 0$ (red) and $9\pi/41$ (blue) relative to the momentum at the conduction-band maximum

6 Conclusion

ARPES measurements on EuB_6 in an extended BZ show unambiguously that the B 2*p* band crosses E_F, thus proving that EuB_6 is a semimetal. Temperature-dependent ARPES spectra show clear exchange-split bands in the FM phase, and even in the PM phase, they show an exchange-driven diffuse structure near E_F, which provides evidence for the formation of MPs. Such spectral behavior is supported by the results of Monte Carlo simulations of ARPES spectra for a 2D Kondo-lattice model.

Acknowledgements We appreciate helpful discussions with B. I. Min, E. J. Choi, J. D. Denlinger, and J. W. Allen. HDK was supported by a National Research Foundation of Korea (NRF) grant funded by the Ministry of Science and ICT (no. NRF-2021R1F1A1063881) and BK and BGC by Gwangju Institute of Science and Technology in 2021 and by NRF (No. NRF-2017R1A2B2008538).

References

1. C.N. Guy, S. von Molnar, J. Etourneau, Z. Fisk, Solid State Commun. **33**, 1055 (1980)
2. L. Degiorgi, E. Felder, H.R. Ott, J.L. Sarrao, Z. Fisk, Phys. Rev. Lett. **79**, 5134 (1997)
3. M. Sigrist, H. Tsunetsugu, K. Ueda, Phys. Rev. Lett. **67**, 2211 (1991)
4. S. Massidda, A. Continenza, T.M. de Pascale, R. Monnier, Z. Phys. B **102**, 83 (1997)
5. J. Kuneš, W.E. Pickett, Phys. Rev. B **69**, 165111 (2004)
6. J.H. Shim, U. Yu, B.I. Min, J. Magn. Magn. Mater. **304**, e346–e348 (2006)
7. R.G. Goodrich, N. Harrison, J.J. Vuillemin, A. Teklu, D.W. Hall, Z. Fisk, D. Young, J. Sarrao, Phys. Rev. B **58**, 14896 (1998)
8. M.C. Aronson, J.L. Sarrao, Z. Fisk, M. Whitton, B.L. Brandt, Phys. Rev. B **59**, 4720 (1999)
9. J.-H. Kim, Y. Lee, C.C. Homes, J.-S. Rhyee, B.K. Cho, S.-J. Oh, E.J. Choi, Phys. Rev. B **71**, 075105 (2005)
10. J. Kim, Y.-J. Kim, J. Kuneš, B.K. Cho, E.J. Choi, Phys. Rev. B **78**, 165120 (2008)
11. X. Zhang, S. von Molnár, Z. Fisk, P. Xiong, Phys. Rev. Lett. **100**, 167001 (2008)
12. J. Kim, W. Ku, C.-C. Lee, D.S. Ellis, B.K. Cho, A.H. Said, Y. Shvyd'ko, Y.-J. Kim, Phys. Rev. B **87**, 155104 (2013)
13. H.J. Tromp, P. van Gelderen, P.J. Kelly, G. Brocks, P.A. Bobbert, Phys. Rev. Lett. **87**, 016401 (2001)
14. J.D. Denlinger, J.A. Clack, J.W. Allen, G.-H. Gweon, D.M. Poirier, C.G. Olson, J.L. Sarrao, A.D. Bianchi, Z. Fisk, Phys. Rev. Lett. **89**, 157601 (2002)
15. S. Souma, H. Komatsu, T. Takahashi, R. Kaji, T. Sasaki, Y. Yokoo, J. Akimitsu, Phys. Rev. Lett. **90**, 027202 (2003)
16. A. Hasegawa, A. Yanase, J. Phys. C Solid State Phys. **12**, 5431 (1979)
17. B. Amsler, Z. Fisk, J.L. Sarrao, S. von Molnar, M.W. Meisel, F. Sharifi, Phys. Rev. B **57**, 8747 (1998)
18. M. Neupane, N. Alidoust, I. Belopolski, G. Bian, S.-Y. Xu, D.-J. Kim, P.P. Shibayev, D.S. Sanchez, H. Zheng, T.-R. Chang, H.-T. Jeng, P.S. Riseborough, H. Lin, A. Bansil, T. Durakiewicz, Z. Fisk, M.Z. Hasan, Phys. Rev. B **92**, 104420 (2015)
19. S.-Y. Gao, S. Xu, H. Li, C.-J. Yi, S.-M. Nie, Z.-C. Rao, H. Wang, Q.-X. Hu, X.-Z. Chen, W.-H. Fan, J.-R. Huang, Y.-B. Huang, N. Pryds, M. Shi, Z.-J. Wang, Y.-G. Shi, T.-L. Xia, T. Qian, H. Ding, Phys. Rev. X **11**, 021016 (2021)
20. W.L. Liu, X. Zhang, S.M. Nie, Z.T. Liu, X.Y. Sun, H.Y. Wang, J.Y. Ding, L. Sun, Z. Huang, H. Su, Y.C. Yang, Z.C. Jiang, X.L. Lu, J.S. Liu, Z.H. Liu, S.L. Zhang, H.M. Weng, Y.F. Guo, Z.J. Wang, D.W. Shen, Z. Liu, arXiv:2103.04658v1 [cond-mat.mtrl-sci]
21. S. Süllow, I. Prasad, M.C. Aronson, J.L. Sarrao, Z. Fisk, D. Hristova, A.H. Lacerda, M.F. Hundley, A. Vigliante, D. Gibbs, Phys. Rev. B **57**, 5860 (1998)
22. P. Nyhus, S. Yoon, M. Kauffman, S.L. Cooper, Z. Fisk, J. Sarrao, Phys. Rev. B **56**, 2717 (1997)
23. C.S. Snow, S.L. Cooper, D.P. Young, Z. Fisk, A. Comment, J.-P. Ansermet, Phys. Rev. B **64**, 174412 (2001)
24. W. Henggeler, H.-R. Ott, D.P. Young, Z. Fisk, Solid State Commun. **108**, 929 (1998)
25. S. Süllow, I. Prasad, M.C. Aronson, S. Bogdanovich, J.L. Sarrao, Z. Fisk, Phys. Rev. B **62**, 11626 (2000)
26. M.L. Brooks, T. Lancaster, S.J. Blundell, W. Hayes, F.L. Pratt, Z. Fisk, Phys. Rev. B **70**, 020401 (2004)
27. R.R. Urbano, P.G. Pagliuso, C. Rettori, S.B. Oseroff, J.L. Sarrao, P. Schlottmann, Z. Fisk, Phys. Rev. B **70**, 140401 (2004)
28. X. Zhang, L. Yu, S. von Molnár, Z. Fisk, P. Xiong, Phys. Rev. Lett. **103**, 106602 (2009)
29. P. Das, A. Amyan, J. Brandenburg, J. Müller, P. Xiong, S. von Molnár, Z. Fisk, Phys. Rev. B **86**, 184425 (2012)
30. U. Yu, B.I. Min, Phys. Rev. Lett. **94**, 117202 (2005)
31. U. Yu, B.I. Min, Phys. Rev. B **74**, 094413 (2006)
32. J.-S. Rhyee, J.Y. Kim, B.K. Cho, H.J. Lee, H.C. Kim, H.M. Park, Phys. Rev. B **74**, 235114 (2006)
33. J.J. Yeh, I. Lindau, At. Data Nucl. Data Tables **32**, 1 (1985)
34. B. Kim, A.B. Andrews, J.L. Erskine, K.J. Kim, B.N. Harmon, Phys. Rev. Lett. **68**, 1931 (1992)
35. M. Kreissl, W. Nolting, Phys. Rev. B **72**, 245117 (2005)
36. W. Nolting, Phys. Rev. B **32**, 403 (1985)